Structural, Electronic, and Thermoelectric Properties of BiSb Nanotubes

H. Y. Lv,[†] H. J. Liu,*[,†] L. Pan,[†] Y. W. Wen,[†] X. J. Tan,[†] J. Shi,*[,†] and X. F. Tang[‡]

Key Laboratory of Artificial Micro- and Nano-structures of Ministry of Education and School of Physics and Technology, Wuhan University, Wuhan 430072, China, and State Key Laboratory of Advanced Technology for Materials Synthesis and Processing, Wuhan University of Technology, Wuhan 430072, China

Received: August 30, 2010; Revised Manuscript Received: October 10, 2010

The structural, electronic, and thermoelectric properties of BiSb nanotubes are investigated using a multiscale approach which combines the first-principles pseudopotential method, semiclassic Boltzmann theory, and molecular dynamics (MD) simulations. Our calculations indicate that the gear-like nanotubes (g-NTs) are energetically more favorable than their hexagonal counterparts (h-NTs). All the g-NTs are found to be semiconducting and their electronic transport coefficients are calculated within the relaxation time approximation. At room temperature, the Seebeck coefficients exhibit obvious peaks near the band edge and their absolute values are very large and increase monotonically with increasing band gaps of the nanotubes. The MD simulations show that the investigated BiSb nanotubes have very low lattice thermal conductivity. The significantly enhanced *ZT* value suggests that by appropriate doping the BiSb nanotubes could be excellent candidates for the thermoelectric applications.

1. Introduction

Since the discovery of carbon nanotubes (CNTs),[1] one-dimensional nanostructures have attracted great interest due to their unusual properties and potential applications in many fields. In particular, nanostructures have played a significant role in the development of high-performance thermoelectric materials. The efficiency of thermoelectric materials is given by the dimensionless figure of merit $ZT = S^2\sigma T/(\kappa_e + \kappa_l)$, where S is the Seebeck coefficient, σ is the electrical conductivity, T is the absolute temperature, and κ_e and κ_l are the electronic and lattice thermal conductivity, respectively. How to enhance the *ZT* value is a key point in the application of thermoelectric materials. During the past 50 years, the Bi-based compounds are found to be promising thermoelectric materials which have a *ZT* value of about 1 at room temperature.[2−4] In 1993, Hicks et al. theoretically predicated that two- and one-dimensional structures could have much larger *ZT* values than the corresponding bulk materials.[5,6] The improvement of thermoelectric efficiency in the low-dimensional systems can be attributed to the enhanced power factor ($PF = S^2\sigma$) caused by a sharper density of states near the Fermi level, as well as the reduced lattice thermal conductivity caused by the increased phonon scattering. Since then, much effort has been made to experimentally synthesize the Bi-based low-dimensional materials. Among them, the $Bi_{1-x}Sb_x$ thin films,[7−9] nanowires,[10−13] and nanotubes[14] have been successfully produced and their enhanced thermoelectric performances have been suggested. On the theoretical side, the Bi nanowires,[15,16] nanotubes,[16−18] and the BiSb nanowires with superlattice and core−shell structures[19] have been systematically studied by first-principles calculations. Most of the investigated systems have the same crystal structure as the Bi or BiSb alloy and are oriented along some particular directions.

Very recently, Teweldebrhan et al. have successfully disassembled Bi_2Te_3 crystal into its building blocks, the Te−Bi−Te−Bi−Te atomic 5-folds, and obtained the atomically thin crystalline films and ribbons of bismuth telluride. The prepared two-dimensional systems are reported to have high electrical conductivity and low thermal conductivity.[20,21] The bulk Bi has a similar pseudolayered structure as Bi_2Te_3, that is, one Bi atom is connected to three nearest neighbors and forms a trigonal pyramid. These pyramids further form a buckled layer by vertex-sharing. The closest distance between neighbor Bi atoms in the same layer is 3.07 Å with covalent bonds. The interactions between adjacent layers are much weaker, and it is reasonable to expect that a layered structure can be disassembled from the bulk Bi under certain experimental conditions. Likewise, one can obtain the BiSb layer from the bulk BiSb alloy in which each Bi atom is covalently connected to the three nearest Sb atoms. In analogy with carbon nanotubes, the BiSb nanotube can be viewed as rolling such a BiSb layer into a cylinder so that the structure is quasi-one-dimensional. It should be noted that Su et al.[17] have studied the electronic properties of Bi nanotubes with such atomic configuration using first-principles calculations.

In this work, we use a multiscale approach to investigate the structural, electronic, and thermoelectric properties of BiSb nanotubes. First, the structural stabilities and electronic properties are studied using a first-principles pseudopotential method. The electronic transport properties are then calculated using the semiclassic Boltzmann theory and rigid-band approximation. In the end, we construct the classical interatomic potentials for BiSb nanotubes by fitting first-principles total energy calculations and calculate the lattice thermal conductivity using molecular dynamics (MD) simulations. We shall see that the *ZT* value of BiSb nanotubes can be very high which suggests their promising thermoelectric applications.

* To whom correspondence should be addressed, phlhj@whu.edu.cn and jshi@whu.edu.cn.

[†] Key Laboratory of Artificial Micro- and Nano-structures of Ministry of Education and School of Physics and Technology, Wuhan University.

[‡] State Key Laboratory of Advanced Technology for Materials Synthesis and Processing, Wuhan University of Technology.

10.1021/jp108231j
Published on Web 11/16/2010

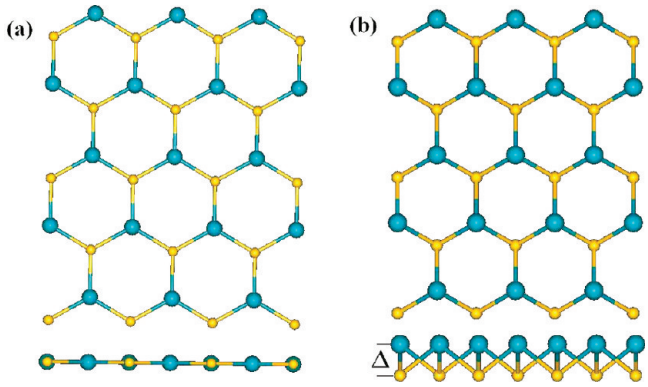

Figure 1. Ball-and-stick model of the (a) planar and (b) buckled BiSb layers. Big blue balls represent Bi atoms, while small yellow balls represent Sb atoms. Both the top and side views are shown.

2. Computational Details

Our first-principles calculations have been performed using a plane-wave pseudopotential formulation[22−24] within the framework of density functional theory (DFT). The exchange-correlation energy is in the form of Perdew−Burke−Ernzerhof (PBE)[25] with generalized gradient approximation (GGA). Since Bi and Sb atoms are both heavy elements, the spin−orbit coupling is considered in the calculations. We adopt a standard supercell geometry[26] so that the BiSb layers/tubes are aligned in a hexagonal array. The closest distance between the layer/tube and its periodic images is set to be 12 Å so that they can be treated as independent entities. The **k** points are sampled on a uniform grid in the BiSb layers or along the BiSb tube axis. Optimal atomic positions are determined until the magnitude of the forces acting on all atoms becomes less than 0.05 eV/Å. On the basis of the calculated band structure, the electronic transport coefficients can be derived by using the semiclassical Boltzmann theory[27] and relaxation time approximation. Within this method, the Seebeck coefficient S is independent of the relaxation time (τ), while the electrical conductivity σ, the electronic component of thermal conductivity κ_e, and the power factor $S^2\sigma$ can only be evaluated with respect to the parameter τ. The lattice component of thermal conductivity κ_l is predicted using equilibrium molecular dynamics (EMD) simulations combined with the Green−Kubo autocorrelation decay method.[28,29] The time step is chosen as 0.55 fs, and 3300 ps raw heat current data are collected to calculate the heat current autocorrelation function.

3. Results and Discussion

We begin our discussions with a buckled layer of BiSb. As mentioned above, this structure can be obtained from the bulk BiSb alloy. Figure 1 is a ball-and-stick model of the buckled layer. For comparison, the planar BiSb layer is also shown which is similar to a graphene sheet. In the planar structure, each Bi atom is covalently connected with three Sb atoms with identical bond length of 3.00 Å and bond angle of 120°. For the buckled layer, the corresponding values are 2.99 Å and 91°. The buckling distance Δ denoted in Figure 1b is found to be 1.69 Å. By rolling the planar and buckled layers, one can obtain the hexagonal (h-) and gearlike (g-) BiSb nanotubes (NTs), respectively. It should be mentioned that there exist two different atomic configurations of g-NTs. For the type I g-NTs, all the Bi atoms form the inner layer and Sb atoms form the outer one. It is just reverse for the type II g-NTs. These three kinds of BiSb nanotubes are illustrated in Figure 2, where both the top and side views are shown. We find that for the g-NTs, the average length of Bi−Sb bonds "along" the tube axis is a little shorter than those bonds wrapping "around" the tube circumference, which is due to the curvature effect and is very similar to that of CNTs.[30] Moreover, the distances between the inner and outer layers of g-NTs are in the range of 1.65−1.75 Å, which is approximately equal to the buckling distance Δ of the buckled BiSb layer.

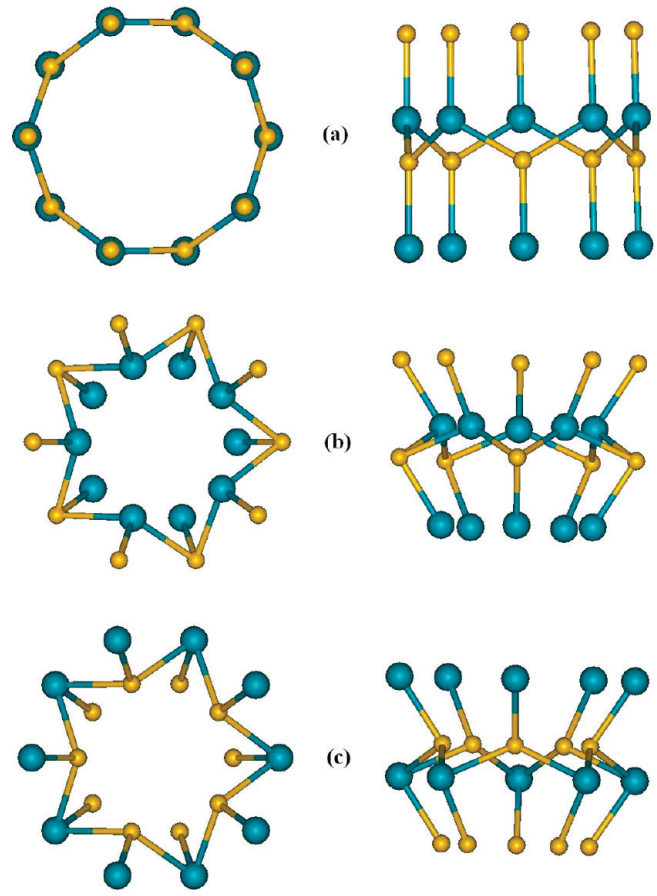

Figure 2. Three kinds of atomic configurations of BiSb nanotubes: (a) h-NT, (b) type I g-NT, and (c) type II g-NT. Both the top and side views are shown.

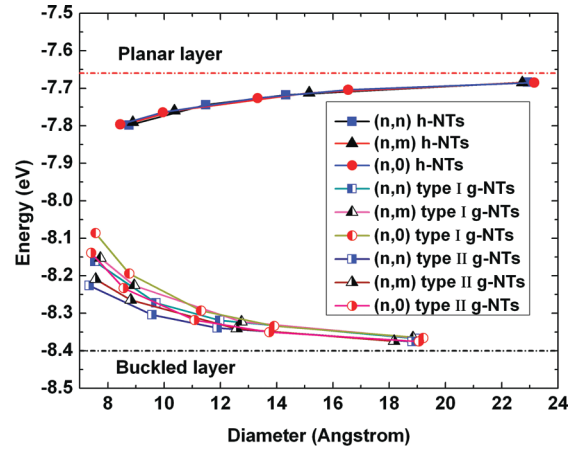

Figure 3. Calculated total energies (in units of eV/Bi−Sb atoms) of three kinds of BiSb nanotubes as a function of tube diameters. For each kind, the armchair, chiral, and zigzag tubes are considered.

Figure 3 plots the total energies of BiSb nanotubes as a function of tube diameters, where both the h-NTs and g-NTs are considered. For comparison, the results of the corre-

TABLE 1: Calculated Total Energies E (in units of eV/Bi−Sb atoms) and Band Gaps E_g (in units of eV) of Three Kinds of BiSb Nanotubes with Different Diameters D and Chiralities

	h-NTs			type I g-NTs			type II g-NTs		
	D	E	E_g	D	E	E_g	D	E	E_g
(3, 3)	8.75	−7.80	0.13	7.54	−8.16	0.42	7.34	−8.23	0.26
(4, 4)	11.48	−7.74		9.71	−8.27	0.58	9.57	−8.30	0.31
(5, 5)	14.33	−7.72	0.04	11.98	−8.32	0.68	11.89	−8.34	0.41
(8, 8)	22.92	−7.68	0.01	18.93	−8.37	0.59	18.81	−8.38	0.49
(4, 2)	8.89	−7.79		7.73	−8.15	0.37	7.57	−8.21	0.02
(5, 2)	10.36	−7.76	0.09	8.93	−8.23	0.55	8.81	−8.27	0.24
(8, 2)	15.16	−7.71		12.75	−8.32	0.66	12.58	−8.34	0.44
(12, 3)	22.74	−7.69	0.01	18.85	−8.37	0.55	18.18	−8.37	0.49
(5, 0)	8.45	−7.80	0.21	7.56	−8.09	0.72	7.41	−8.14	0.48
(6, 0)	9.96	−7.76	0.23	8.76	−8.19	0.79	8.57	−8.23	0.62
(8, 0)	13.33	−7.73	0.11	11.32	−8.29	0.74	11.08	−8.32	0.53
(10, 0)	16.54	−7.70	0.14	13.91	−8.33	0.65	13.74	−8.35	0.51
(14, 0)	23.16	−7.69		19.21	−8.37	0.54	19.06	−8.38	0.47

sponding planar and buckled layers are also indicated. We see that the energies of h-NTs increase monotonically with increasing diameters and finally approach to the value of planar BiSb layer. It is interesting to note that the energies of h-NTs only depend on the tube diameter and there is no chirality dependence. By fitting the calculated values, the energy of a h-NT can be approximately expressed as $E = -0.624e^{-d/5.159} - 7.678$, where d is the tube diameter. The picture is however quite different for the g-NTs. As can be seen from Figure 3, the energies of both type I and type II g-NTs are lower than those of h-NTs and decrease with increasing diameters and finally approach to the energy of buckled BiSb layer. At relatively smaller diameter, the energies of type II g-NTs are a bit lower than those of the corresponding type I g-NTs. There is a weak chirality dependence of the total energies for both type I and type II g-NTs, that is, the energy is highest for the zigzag BiSb nanotube, lowest for the armchair nanotube, with the chiral nanotube in between. However, when the tube diameters are increased, these energy differences become smaller and smaller and finally all the energies approach that of the BiSb buckled layer.

We have also calculated the electronic properties of these h-NTs and g-NTs with different diameters and chiralities. It is found that almost all the investigated BiSb nanotubes are semiconducting and the corresponding band gaps are summarized in Table 1. We see that the band gaps of g-NTs are obviously larger than those of the h-NTs with the same diameter and chirality, and the band gaps of the type I g-NTs are on the other hand larger than those of the type II g-NTs. As shown in Figure 4, the band structures of BiSb nanotubes are very sensitive to their atomic configurations. In particular, all the semiconducting h-NTs have indirect band gaps (see Figure 4a−c). This is however not the case for the g-NTs. We see from Figure 4d that as the diameter increases, the valence band maximum (VBM) of type I g-NTs (n, n) slowly moves away from the Γ point while the conduction band minimum (CBM) moves toward the Γ point, which exhibits a transition of indirect−direct−indirect band gaps. The VBM of type II g-NTs (n, n) (Figure 4g) has similar behavior as their type I counterparts (Figure 4d); however, the CBM does not move toward the Γ point with increasing diameter, thus all type II g-NTs (n, n) are indirect-band-gap semiconductors. As for the g-NTs (n, m), we see from parts e and h of Figure 4 that all of them have indirect band gaps where the VBM is a little away from the Γ point. On the other hand, we see from parts f and i of Figure 4 that the type I g-NTs (n, 0) change from indirect- to direct-band-gap semiconductors with increasing diameters, while all the type II g-NTs (n, 0) exhibit indirect band gaps.

We now move to the discussions of transport properties of BiSb nanotubes. Here we focus on the type II g-NTs since they are energetically more favorable than the corresponding h-NTs and type I g-NTs. On the basis of the above-mentioned band structures, we are able to evaluate the transport coefficients by using the semiclassical Boltzmann theory[27] and the rigid-band approach.[31] Figure 5 shows the calculated Seebeck coefficients S and power factors $S^2\sigma$ as a function of chemical potential μ at 300 K. Note here the power factors are evaluated with respect to the relaxation time. Within the rigid-band approach, the chemical potential indicates the doping level of the system. In the case of p-type doping, the Fermi level gets down-shifted corresponding to $\mu < 0$. For n-type doping, the Fermi level shifts up and $\mu > 0$. As can be seen from Figure 5a, the Seebeck coefficients of (n, n) tubes have two peaks around the Fermi level ($\mu = 0$), and the peak values at $\mu > 0$ are relatively larger than those at $\mu < 0$ and reach a maximum (absolute) value of 794.6 μV/K at $\mu = 0.038$ eV for the investigated armchair tubes. In contrast, there are several peaks around the Fermi level for the Seebeck coefficients of (n, m) tubes (see Figure 5b). The maximum Seebeck coefficient for the considered chiral tubes is 763.0 μV/K at $\mu = -0.043$ eV. As for the (n, 0) tubes, there also exhibit two peaks in the calculated Seebeck coefficients around the Fermi level (see Figure 5c). Among the investigated zigzag tubes, we see that the (6, 0) has the largest Seebeck coefficient with the absolute value of 969.9 μV/K at $\mu = 0.046$ eV. One may wonder if there is a relation between the diameters and the Seebeck coefficients of these BiSb nanotubes. However, if we focus on the calculated band gaps (Table 1), we find that for all the three kinds of nanotubes, the absolute peak values of Seebeck coefficients actually increase with increasing band gaps. This is consistent with previous reports as long as the doping level is not very high.[32] It should be mentioned that compared with other Bi-based systems, these BiSb nanotubes exhibit much larger Seebeck coefficients, which is very beneficial for their thermoelectric applications.

Parts d−f of Figure 5 plot the power factors ($S^2\sigma$) as a function of chemical potential (μ) at 300 K for these BiSb nanotubes, where the relaxation time τ is included as a parameter. We find that for all the investigated nanotubes, there exist obviously sharp peaks around the Fermi level, which indicates that the power factors of these nanotubes can be largely optimized by proper doping. Within the rigid-band picture, the optimal doping concentration can be obtained by integrating the density of states of these nanotubes from the Fermi level to the desired chemical potential.[33] We further find that the (n, 0) and (n, n) tubes generally have larger peak values of the power factors than those of the (n, m) tubes. On the other hand, we see from Figure 5e that for the (4, 2) and (5, 2) tubes which have relatively smaller band gaps, there exist more than one sharp peak both below and above the Fermi level. This observation may result from large oscillations of their Seebeck coefficients and is very different from those tubes with larger band gaps.

To study the thermal transport properties of the BiSb nanotubes, we have performed classical MD simulations where suitable interatomic potentials are needed. However, as far as we are aware, there have not been any available empirical potential for the nanostructures of BiSb. Considering that the

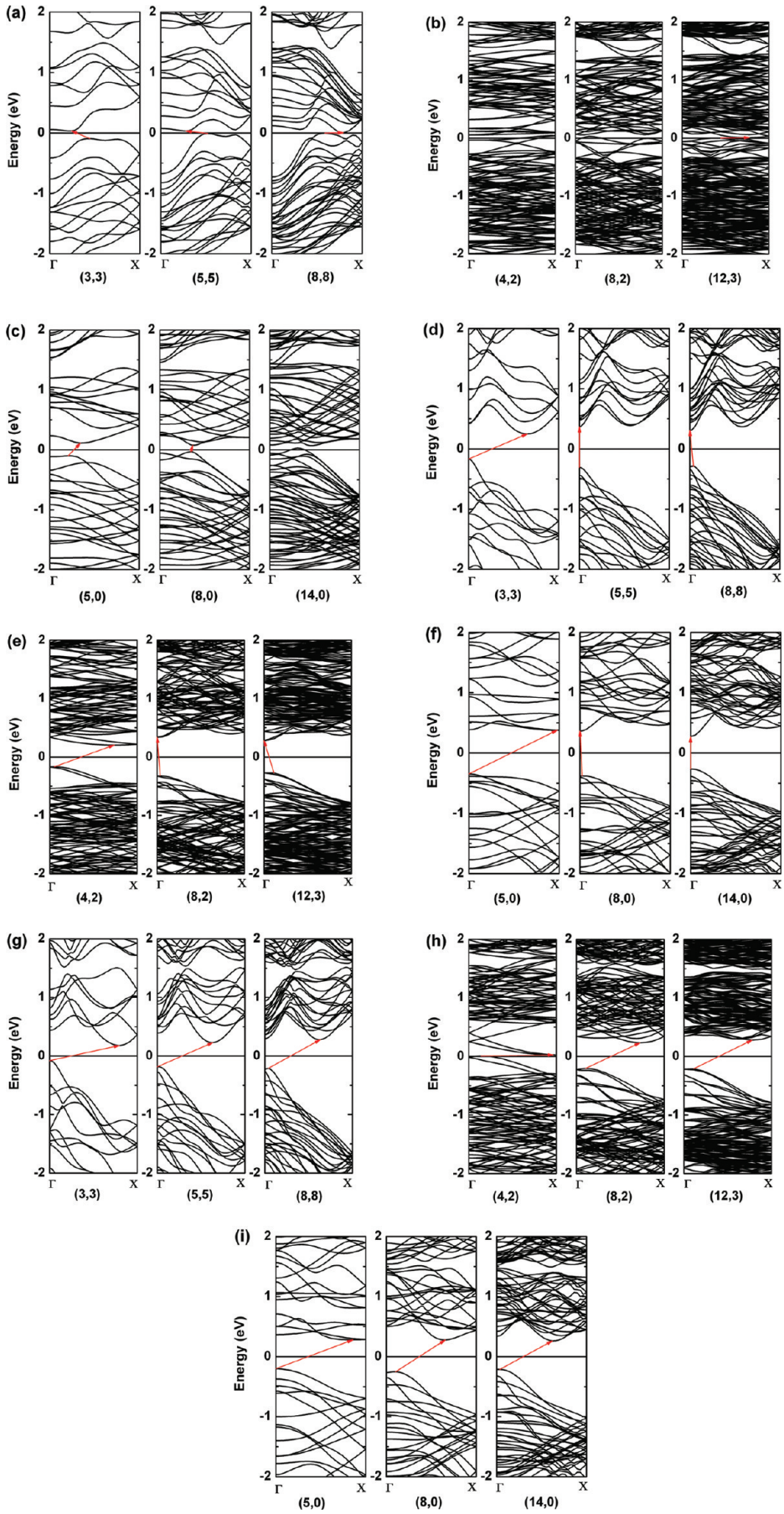

Figure 4. Calculated energy band structures of (a) armchair h-NTs, (b) chiral h-NTs, (c) zigzag h-NTs, (d) armchair g-NTs of type I, (e) chiral g-NTs of type I, (f) zigzag g-NTs of type I, (g) armchair g-NTs of type II, (h) chiral g-NTs of type II, and (i) zigzag g-NTs of type II. The red arrows indicate that the band gap is direct or indirect.

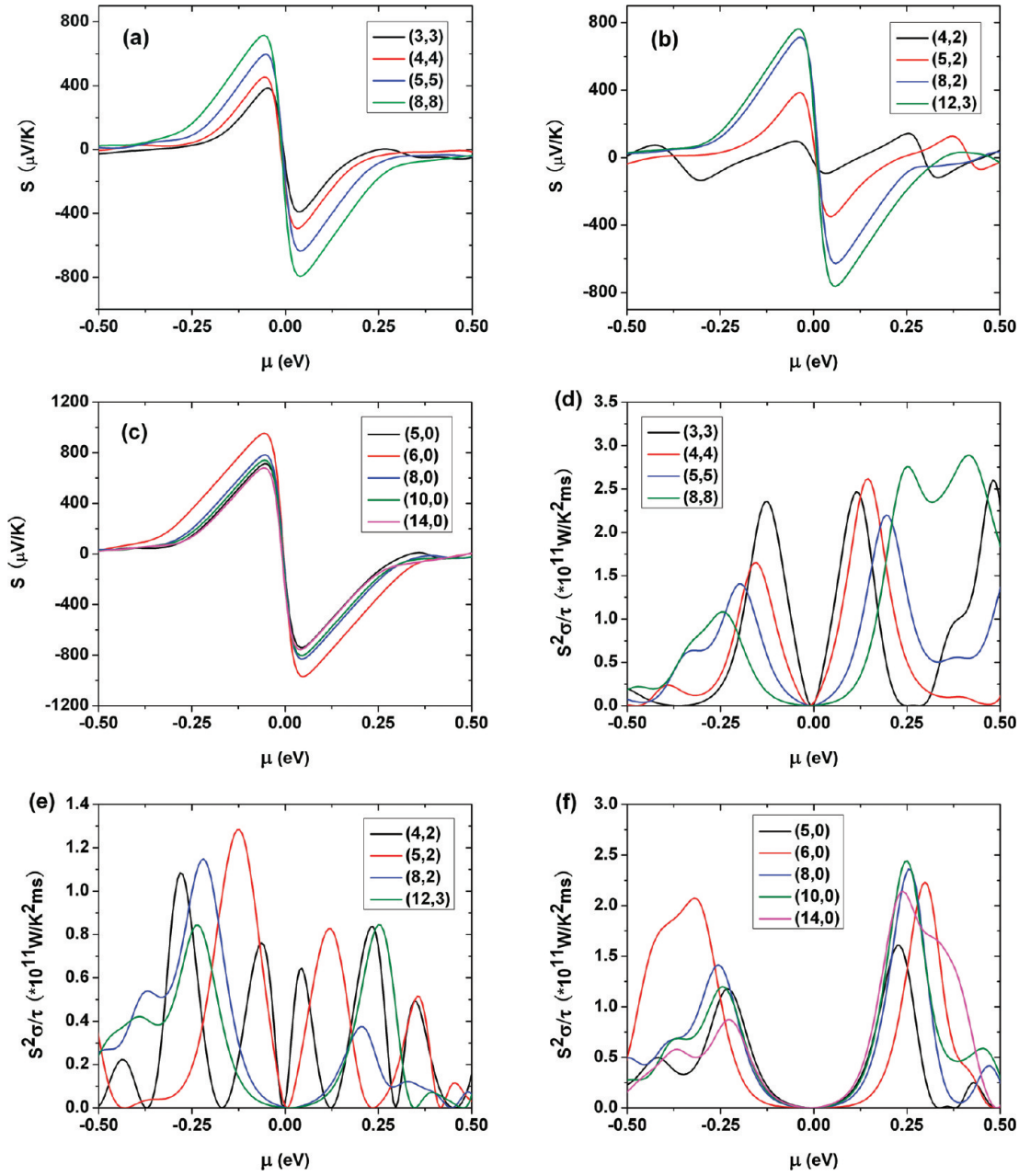

Figure 5. Calculated Seebeck coefficients at 300 K as a function of chemical potential for type II g-NTs with different diameters and chiralities: (a) armchair (n, n), (b) chiral (n, m), and (c) zigzag (n, 0). The calculated power factors for these BiSb nanotubes are shown in (d), (e), and (f), respectively. Note (d), (e), and (f) are evaluated with respect to the relaxation time τ.

interatomic interactions in the BiSb nanotubes are mainly of short range, we employ a simple two-body Morse potential which includes the anharmonic interactions and is found to predict the lattice thermal conductivity quite well.[34] The Morse potential is in the form of $\varphi(r_{ij}) = D_e\{[1 - e^{-a(r_{ij}-r_0)}]^2 - 1\}$, where D_e is the depth of the potential well, a is the measure of bond elasticity, r_{ij} is the interatomic separation between atom i and j, and r_0 is the equilibrium bond distance. The parameters in the Morse potential can be determined by fitting the energy surface from first-principles calculations.[32,34] The energy surface is scanned by changing the tube diameters, the distances between the inner and outer walls, and the periodic lengths along the tube axis to obtain a series of distinct configurations. The fitting procedure is done by using the so-called GULP code.[35] Here we take type II g-NT (5, 0) as an example and the optimal parameters in the Morse potential are listed in Table 2. It is obvious that the Bi−Sb bond has a much higher bonding energy than that of the Bi−Bi and Sb−Sb bonds. On the other hand, the Bi−Bi bond is a bit stronger than the Sb−Sb bond.

TABLE 2: Fitted Parameters in the Morse Potential for the Type II g-NT (5, 0)[a]

interaction	D_e (eV)	a (1/ Å)	r_0 (Å)	r_c (Å)
Bi−Sb	2.510	0.940	3.11	4.5
Bi−Bi	0.294	1.960	4.11	6.0
Sb−Sb	0.115	1.540	3.52	4.5

[a] Here D_e is the depth of the potential well, a is the measure of bond elasticity, r_c is the equilibrium bond distance, and r_c is the cutoff distance.

Based on the MD simulations, the lattice thermal conductivity κ_l can be predicted by using the Green−Kubo expression

$$\kappa_{\mu\nu}(\tau_{\mathrm{m}}) = \frac{1}{Vk_{\mathrm{B}}T^2}\int_0^{\tau_m}\langle J_\mu(\tau)J_\nu(0)\rangle\,\mathrm{d}\tau$$

Here $\langle J_\mu(\tau)J_\nu(0)\rangle$ is the heat current autocorrelation function, V is the volume of the simulation system, κ_{B} is the Boltzmann constant, and T is the system temperature. For a pair potential, the heat current $\vec{J}(t)$ can be expressed as

$$\vec{J}(t) = \sum_i \varepsilon_i\vec{v}_i + \frac{1}{2}\sum_{i,j\neq i}(\vec{F}_{ij}\cdot\vec{v}_i)\vec{r}_{ij}$$

where ε_i is the site energy of atom i, $\vec{v}_i$ is the corresponding velocity, $\vec{F}_{ij}$ is the force between atom i and j, and $\vec{r}_{ij}$ is their separation. For the type II g-NT (5, 0), our calculated thermal conductivity is 0.53 W/(m K) at room temperature. Simulations for other BiSb tubes also find very low values of the lattice thermal conductivity which is quite desirable for their thermoelectric applications.

To evaluate the figure of merit ZT, we have to determine the relaxation time τ which is included in the power factor as a parameter. The accurate treatment of the relaxation time depends on the exact doping atoms used in the experiments and the detailed scattering mechanism. Here we just give a reasonable estimation of τ. It is believed that near room temperature, the electronic thermal conductivity of Bi-based nanostructures can compete with that from the lattice.[18,36,37] By assuming $\kappa_{\mathrm{e}} = \kappa_{\mathrm{l}}$ and comparing the κ_{e}/τ calculated using the Boltzmann theory, the relaxation time τ is readily obtained. For the type II g-NT (5, 0), the calculated value is $\tau = 1.3 \times 10^{-12}$ s, which is larger by 2 orders of magnitude than that of most Bi-based bulk materials.[33,38,39] It should be mentioned that this large τ is only applicable for the pristine BiSb nanotube. Even if the relaxation time would be reduced by an order of magnitude when the tube is doped, we can still get a ZT value of about 6 at the optimized doping level mentioned above ($\mu = 0.23$ eV, see Figure 5f). Such a high figure of merit suggests that by appropriate doping, the BiSb nanotubes should be very promising thermoelectric materials which needs future experimental investigation.

4. Summary

In summary, we have performed multiscale computations to study the thermoelectric properties of BiSb in several nanotube structures. At electronic scale, the energy band structures of these nanostructures are investigated using first-principles calculations. The electronic transport coefficients are then calculated within the Boltzmann theory. At atomic scale, the lattice thermal conductivity is predicated by equilibrium molecular dynamics, where the parameters in the Morse potential are obtained by fitting the total energy calculations at electronic scale. Our theoretical results give the possibility to use BiSb nanotubes as high performance thermoelectric materials.

Acknowledgment. This work was supported by the "973 Program" of China (Grant No. 2007CB607501), the Program for New Century Excellent Talents in University, and the Natural Science Foundation for the Outstanding Young Scientists of Hubei Province. We are also grateful for financial support from the "Fundamental Research Funds for the Central Universities". All the calculations were performed in the PC Cluster from Dawn Company of China.

References and Notes

(1) Iijima, S. *Nature* **1991**, *354*, 56.
(2) *CRC Handbook of Thermoelectrics*; Rowe, D. M., Ed.; CRC Press: Boca Raton, FL, 1995.
(3) Tritt, T. *Science* **1999**, *283*, 804.
(4) DiSalvo, F. J. *Science* **1999**, *285*, 703.
(5) Hicks, L. D.; Dresselhaus, M. S. *Phys. Rev. B* **1993**, *47*, 12727.
(6) Hicks, L. D.; Dresselhaus, M. S. *Phys. Rev. B* **1993**, *47*, 16631.
(7) Cho, S.; DiVenere, A.; Wong, G. K.; Ketterson, J. B.; Meyer, J. R. *Phys. Rev. B* **1999**, *59*, 10691.
(8) Cho, S.; Kim, Y.; DiVenere, A.; Wong, G. K. L.; Ketterson, J. B.; Meyer, J. R. *J. Appl. Phys.* **2000**, *88*, 808.
(9) Biçer, M.; Köse, H.; Şişman, İ. *J. Phys. Chem. C* **2010**, *114*, 8256.
(10) Lin, Y. M.; Cronin, S. B.; Rabin, O.; Ying, J. Y.; Dresselhaus, M. S. *Appl. Phys. Lett.* **2001**, *79*, 677.
(11) Lin, Y. M.; Rabin, O.; Cronin, S. B.; Ying, J. Y.; Dresselhaus, M. S. *Appl. Phys. Lett.* **2002**, *81*, 2403.
(12) Zhang, Y.; Li, L.; Li, G. H. *Nanotechnology* **2005**, *16*, 2096.
(13) Dou, X. C.; Li, G. H.; Lei, H. C. *Nano Lett.* **2008**, *8*, 1286.
(14) Dou, X. C.; Li, G. H.; Huang, X. H.; Li, L. *J. Phys. Chem. C* **2008**, *112*, 8167.
(15) Lin, Y. M.; Sun, X. Z.; Dresselhaus, M. S. *Phys. Rev. B* **2000**, *62*, 4610.
(16) Qi, J. S.; Shi, D. N.; Zhao, J. J.; Jiang, X. F. *J. Phys. Chem. C* **2008**, *112*, 10745.
(17) Su, C. R.; Liu, H. T.; Li, J. M. *Nanotechnology* **2002**, *13*, 746.
(18) Zhou, G.; Li, L.; Li, G. H. *Appl. Phys. Lett.* **2010**, *97*, 023112.
(19) Qi, J. S.; Shi, D. N.; Chen, H. X.; Wang, B. L. *J. Phys. Chem. C* **2009**, *113*, 11358.
(20) Teweldebrhan, D.; Goyal, V.; Rahman, M.; Balandin, A. A. *Appl. Phys. Lett.* **2010**, *96*, 053107.
(21) Teweldebrhan, D.; Goyal, V.; Balandin, A. A. *Nano Lett.* **2010**, *10*, 1209.
(22) Kresse, G.; Hafner, J. *Phys. Rev. B* **1993**, *47*, 558.
(23) Kresse, G.; Hafner, J. *Phys. Rev. B* **1994**, *49*, 14251.
(24) Kresse, G.; Furthmüller, J. *Comput. Mater. Sci.* **1996**, *6*, 15.
(25) Perdew, J. P.; Burke, K.; Ernzerhof, M. *Phys. Rev. Lett.* **1996**, *77*, 3865.
(26) Blase, X.; Benedict, L. X.; Shirley, E. L.; Louie, S. G. *Phys. Rev. Lett.* **1994**, *72*, 1878.
(27) Madsen, G. K. H.; Singh, D. J. *Comput. Phys. Commun.* **2006**, *175*, 67.
(28) Plimpton, S. *J. Comput. Phys.* **1995**, *117*, 1.
(29) Schelling, P. K.; Phillpot, S. R.; Keblinski, P. *Phys. Rev. B* **2002**, *65*, 144306.
(30) Liu, H. J.; Chan, C. T. *Phys. Rev. B* **2002**, *66*, 115416.
(31) Holland, M. G. *Phys. Rev.* **1963**, *132*, 2461.
(32) Huang, B. L.; Kaviany, M. *Phys. Rev. B* **2008**, *77*, 125209.
(33) Lv, H. Y.; Liu, H. J.; Pan, L.; Wen, Y. W.; Tan, X. J.; Shi, J.; Tang, X. F. *Appl. Phys. Lett.* **2010**, *96*, 142101.
(34) Qiu, B.; Ruan, X. L. *Phys. Rev. B* **2009**, *80*, 165203.
(35) Gale, J.; Rohl, A. *Mol. Simul.* **2003**, *29*, 291.
(36) Moore, A. L.; Pettes, M. T.; Zhou, F.; Shi, L. *J. Appl. Phys.* **2009**, *106*, 034310.
(37) Hasegawa, Y.; Murata, M.; Nakamura, D.; Komine, T. *J. Appl. Phys.* **2009**, *106*, 063703.
(38) Scheidemantel, T. J.; Ambrosch-Draxl, C.; Thonhauser, T.; Badding, J. V.; Sofo, J. O. *Phys. Rev. B* **2003**, *68*, 125210.
(39) Thonhauser, T.; Scheidemantel, T. J.; Sofo, J. O. *Appl. Phys. Lett.* **2004**, *85*, 588.

JP108231J